Atmos. Chem. Phys., 25, 16315–16330, 2025 https://doi.org/10.5194/acp-25-16315-2025 © Author(s) 2025. This work is distributed under the Creative Commons Attribution 4.0 License.





Measurement report: Molecular characterization of organic aerosol in coastal environments using offline FIGAERO-I-CIMS

Yuping Chen^{1,2,3}, Lingling Xu^{1,2}, Xiaolong Fan^{1,2}, Ziyi Lin^{1,2,3}, Chen Yang^{1,2,3}, Gaojie Chen^{1,2,3}, Ronghua Zheng^{1,2}, Youwei Hong^{1,2}, Mengren Li^{1,2}, Yanru Zhang⁴, and Jinsheng Chen^{1,2}

¹State Key Laboratory of Advanced Environmental Technology, Institute of Urban Environment,
Chinese Academy of Sciences, Xiamen 361021, China

²Fujian Key Laboratory of Atmospheric Ozone Pollution Prevention, Institute of Urban Environment, Chinese Academy of Sciences, Xiamen 361021, China

³University of Chinese Academy of Sciences, Beijing 100049, China

⁴Xiamen Environmental Monitoring Station, Xiamen 361021, China

Correspondence: Lingling Xu (linglingxu@iue.ac.cn) and Jinsheng Chen (jschen@iue.ac.cn)

Received: 30 April 2025 – Discussion started: 11 August 2025 Revised: 23 September 2025 – Accepted: 27 October 2025 – Published: 20 November 2025

Abstract. Organic aerosol (OA), as a key component of particulate matter, exerts significant impacts on public health and the environment. However, understanding of molecular characterization of OA under diverse environments remains limited. This study employed offline FIGAERO-I-CIMS (Filter Inlet for Gases and Aerosols coupled with iodide-adduct Chemical Ionization Mass Spectrometry) to analyze the molecular composition of OA in PM_{2.5} samples collected from a coastal city (urban and seaside sites) in Southeast China during spring 2024. A total of 737 and 768 CHOX compounds were identified at the urban and seaside sites, respectively. CHO compounds dominated in signal intensity (> 70 %) at both sites, while CHON were more abundant at the urban site and S-containing compounds at the seaside site. The weighted effective oxygen to carbon content (O_{eff}/C) ratios (urban 0.82, seaside 0.85) indicated the highly oxidized nature of coastal compounds. Seaside CHOX exhibited lower unsaturation, reduced aromaticity, and higher oxidation states. Categorization showed that urban OA was more influenced by aromatic compounds, whereas seaside OA contained higher proportions of aged aliphatic compounds. Two distinct pollution episodes were selected to investigate CHOX evolution. Case 1 (local accumulation) exhibited enhanced CHON signals attributable to increased organonitrate formation under elevated NO_x levels, whereas Case 2 (marine air masses) showed enhanced CHO signals and a higher CHOX oxidation state likely resulting from intensified aqueous/heterogeneous reactions under humid conditions. These findings advance our understanding of OA molecular characteristics and chemical evolution under different environmental conditions.

1 Introduction

The chemical compositions of organic aerosol (OA) are highly complex, exerting distinct impacts on human health and the environment. Parts of OA are emitted directly from natural and anthropogenic sources, known as primary organic aerosols (POA). Additionally, gaseous precursors such as SO₂, NO_x, and volatile organic compounds (VOCs) could

undergo a series of chemical reactions to form secondary organic aerosol (SOA) (Putman et al., 2012; Qi et al., 2017; Xu et al., 2020). Current research has focused more on the quantification and the characteristic of bulk OA (Chazeau et al., 2021; Huang et al., 2014; Sun et al., 2018; Zhou et al., 2020). At the molecular level, OA remains not well understood due to its complex composition, consisting of numerous individual compounds with diverse volatility, function-

ality, and solubility, and its ultralow atmospheric concentration, which introduces large uncertainties in detection and compound-specific identification (Stark et al., 2017; Xu et al., 2017a; Yu et al., 2016; Zheng et al., 2021). Both anthropogenic and natural sources of OA exacerbate the challenge of their identification and quantification in molecular composition (Daellenbach et al., 2024). Several studies have characterized OA in different environments and have found significant variations in its molecular composition (Chen et al., 2020; Siegel et al., 2021; Zhang et al., 2024). A recurring pattern shows that CHO and CHON compounds dominate urban OA, whereas S-containing species are more abundant in marine aerosols. Nevertheless, there has been inadequate research on the molecular characterization of OA under complex conditions, such as the urban-coastal interface. This is particularly true regarding the evolution of OA composition during high PM_{2.5} episodes in such environments. Therefore, detailed molecular-level characterization of OA is essential for advancing the understanding of OA formation mechanisms and providing critical insights into aerosol control strategies (Redman et al., 2002; Wan et al., 2020).

Hard ionization techniques, such as Aerosol Mass Spectrometer (AMS) and Aerosol Chemical Speciation Monitor (ACSM), which are commonly used for online observation of aerosol organic components, cannot provide molecular information of individual compounds. In contrast, soft ionization techniques overcome this limitation by enabling observation of OA molecular compounds. A variety of advanced mass spectrometry techniques, such as two-dimensional Gas Chromatograph-Electron Ionization time-of-flight Mass Spectrometry (GC × GC-EI-ToF-MS), Electrospray Ionization-Fourier Transform Ion Cyclotron Resonance Mass Spectrometry (ESI-FT-ICR MS), Extractive Electrospray Ionization time-of-flight Mass Spectrometry (EESI-TOF MS), and Filter Inlet for Gases and Aerosols-Chemical Ionization Mass Spectrometry equipped with reagent ion iodide (FIGAERO-I-CIMS), have been widely used to characterize OA compositions due to their ultrahigh mass accuracy and resolution (An et al., 2019; Cui et al., 2024; Daellenbach et al., 2024; Lopez-Hilfiker et al., 2019). However, these methods differ in their detection characteristics, including pretreatment procedures, instrumental resolution, and sensitivity toward specific compound classes. Among these, FIGAERO-I-CIMS has proven particularly effective for detecting highly oxidized, acidic, and polar organic species (Lee et al., 2014; Lopez-Hilfiker et al., 2014; Bianchi et al., 2019; Du et al., 2022; Xin et al., 2024). Moreover, FIGAERO-I-CIMS performs direct thermal desorption of filter samples, which reduces potential sample loss or compositional changes associated with conventional pretreatment procedures.

FIGAERO-I-CIMS can operate in both online and offline modes. However, conducting long-term online observation poses significant challenges, particularly in maintaining instrument stability and airtightness. To date, the longest such observation reported was conducted by Daellenbach et al. (2024) in Beijing, which lasted for seven months. Compared to online mode, the offline mode of FIGAERO-I-CIMS lowers operating and maintenance costs and provides greater convenience for detecting samples from different environments within a short period of time. Recent studies have reported the employments of FIGAERO-I-CIMS in offline mode, e.g., at an urban background site during summer and winter in Stuttgart City, Germany (Huang et al., 2019), at an urban site in Beijing, China, under varying pollution levels (Cai et al., 2022), and on the route near the North Pole (Siegel et al., 2021). To date, research on the molecular composition of OA under varying environmental conditions remains quite limited.

In this study, offline FIGAERO-I-CIMS was applied to characterize OA at the molecular level in PM2.5 samples collected from two different sites (urban and seaside) in Xiamen, a coastal city in Southeast China, during spring 2024. Expanding on our earlier ACSM measurement, OA constituted 30 %-60 % of fine aerosol in Xiamen, with SOA accounting for over 70% (Chen et al., 2022; Zhang et al., 2020). This work has three main objectives: (i) to characterize the molecular composition of OA and assess source impacts; (ii) to compare the physicochemical properties of CHOX compounds including saturation, oxidation state, and aromaticity, between urban and seaside environments; and (iii) to elucidate the chemical evolution processes of organic molecules through case studies. The findings will shed light on the influence of emission sources and atmospheric chemical processes on OA molecular composition in different environments.

2 Experimental Methods

2.1 PM_{2.5} Sampling and Offline FIGAERO-I-CIMS Analysis

The study was conducted at two distinct sampling sites (an urban site and a seaside site) in Xiamen, a city situated along the southeast coast of China and characterized by a subtropical marine monsoon climate. The urban site was situated at the Institute of Urban Environment, Chinese Academy of Sciences (24°26′ N, 118°03′ E). This site lies in proximity to major roads (Jimei Avenue and Haixiang Avenue) approximately 100 m away. The seaside site was located at the Xiamen Atmospheric Observation Supersite (24°28′ N, 118°10′ E), approximately 2.5 km from the coastline. Both sites are influenced by anthropogenic and marine sources, though to varying degrees. In terms of human activities, both sites are affected by vehicle emissions, while the urban site is more affected by industrial coal combustion and the seaside site is more affected by port machinery/ship fuel emissions. Regarding marine sources, the seaside site experiences stronger impacts from sea salt and marine biological activities. PM_{2.5} was sampled during the spring season from 20 March to 30 April 2024, with a sampling time of 23 h from 10:00 a.m. to 09:00 a.m. local time (LT) the following day for each sample. A total of 38 and 32 filter samples were obtained from the urban and seaside sites, respectively, with one procedure blank used to assess potential contamination during sampling and transportation.

The offline filter sampling steps are similar to previous studies (Hong et al., 2019, 2022). Briefly, a high-volume aerosol sampler (TH-1000 series, Tianhong Corp., Wuhan, China) was operated at a flow rate of $1.05~{\rm m}^3~{\rm min}^{-1}$ and particulate matter with a diameter of less than $2.5~{\rm \mu m}$ was collected on pre-baked quartz fiber filters ($18~{\rm cm} \times 23~{\rm cm}$). Before sampling, the quartz filters were wrapped in aluminum foil and burned in a muffle furnace for $4~{\rm h}$ (temperature: $450~{\rm cm}$) to remove residual carbon components from the filters. The burned quartz filters were conditioned in a constant temperature ($25~{\rm cm}$) and humidity ($60~{\rm cm}$) chamber for $24~{\rm h}$, and then weighed using a balance. After sampling, the filter samples were stored at $-20~{\rm cm}$ before further chemical analysis. The field blank sample was taken following the same procedure without drawing air through the sampler.

PM_{2.5} filter samples were analyzed by the FIGAERO-CIMS in offline mode with negative iodide (I⁻) ions as the reagent (Aerodyne Research Inc., USA and Tofwerk AG, Switzerland). Heated and dry ultra-high-purity (UHP) N₂ was passed through a permeation tube containing liquid methyl iodide (CH₃I; Alfa Aesar, 99 %) to an X-ray source (Tofwerk AG, P-type), producing I⁻ to charge the thermally desorbed compounds. Different from the sandwich method used in other studies (Cai et al., 2022, 2023; Xin et al., 2024), an area (1.85 cm²) of the sample filters was punched and placed manually in the dedicated filter holder of FIGAERO directly. This larger area of filter membrane was used to enhance mass spectrometry signals due to the relatively low particle concentration in this study. More information was described in Sect. S1. A uniform temperature ramping protocol was applied for all filters, following four steps: (1) stabilization at 25 °C for 1 min; (2) heating from 25 to 200 °C in 24 min; (3) soaking at 200 °C for 15 min; and (4) cooling to 25 °C within 15 min. Two heating cycles were analyzed for each filter sample to assess the instrument background (Fig. S1). Meanwhile, parallel experiments were conducted to evaluate the reproducibility of sampling and analytical procedures. These tests showed excellent agreement between the OA signal intensities of duplicate samples, with linear regression slopes of 0.84–1.13 and correlation coefficients (r^2) upwards to 0.997 (Fig. S2).

2.2 Coordinated Observations

Simultaneous observations of atmospheric species were also carried out at the same stations during the sampling campaign. The method of N_2O_5 concentration detected by online I-CIMS was described by Chen et al. (2024). The concentrations of water-soluble ions, including Na^+ , NH_4^+ , K^+ ,

 Ca^{2+} , Mg^{2+} , F^- , Cl^- , NO_3^{2-} and SO_4^{2-} , were measured by Ion Chromatography (Metrohm 883). OC and EC concentrations were detected by a Model-4 semi-continuous OC / EC aerosol analyzer (Sunset Laboratory Inc., USA). Additional measurements were obtained from instruments deployed at the sampling sites and nearby national air quality monitoring stations, located approximately 1 and 2 km from the IUE and XS, respectively. Trace gases, i.e., carbon oxide (CO), ozone (O_3) , sulfur dioxide (SO_2) , and nitrogen oxides (NO_r) , were simultaneously measured by gas analyzers (Thermo Fisher Scientific, Waltham, MA, USA). Meteorological parameters, including wind speed (WS), wind direction (WD), temperature (T), and relative humidity (RH), were recorded by automatic weather observation station. Ultraviolet radiation (UVB) was determined by a UV radiometer (KIPP & ZO-NEN, SUV5 Smart UV Radiometer). Comprehensive data for all measured parameters at both sites are summarized in Table S1.

2.3 Data Process and Analysis

The TofTools package (Junninen et al., 2010; version 6.11) based on MATLAB (MathWorks Inc.) was used to analyze offline FIGAERO-I-CIMS data. The majority of detected compounds fell within the m/z range of 200–500. These ions formed I⁻ adducts, i.e., [M]I⁻, where M represents the original molecular formula of the analytes. Besides, a small proportion of compounds existed in other forms, such as losing a hydrogen (H) atom and combining with NO₃⁻ or HNO₃I⁻. Mass calibration was performed using five calibrants: NO₃⁻ (m/z 61.99), I⁻ (m/z 126.91), H₂OI⁻ (m/z 144.92), HNO₃I⁻ (m/z 189.90), and I₃⁻ (m/z 380.71).

High-resolution peak fitting was performed on 1 min averaged data, the signal intensity of each compound was subsequently normalized to the signal of reagent I^- and H_2OI^- . Signals of the first 1 min of ramping and the last 1 min of soaking periods were excluded in order to minimize potential interference from temperature transitions (Cai et al., 2023), the calculation formula of the normalized signal for each compound i was as follows:

Normalized_Signal_i =
$$\frac{\int_{t=2}^{t=39} \text{signal}_{i}}{\int_{t=2}^{t=39} \text{signal}_{I^{-}} + \int_{t=2}^{t=39} \text{signal}_{H_{2}\text{OI}^{-}}} - \frac{\int_{t=57}^{t=99} \text{signal}_{i}}{\int_{t=57}^{t=94} \text{signal}_{I^{-}} + \int_{t=57}^{t=94} \text{signal}_{H_{2}\text{OI}^{-}}}$$
(1)

The detected molecules were classified into four categories based on their elemental composition: CHO (containing only C, H, and O elements), CHON (containing 1–2 N atoms in addition to C, H, and O elements), CHOS (containing only C, H, O, and S elements), and CHONS compounds (containing C, H, O, N, and S elements). In this study, CHOS and CHONS were collectively categorized as S-containing compounds. The sum of the four compound classes was denoted

as CHOX, where X indicates the potential presence of N, S, or both.

To characterize the properties of the OA compounds, the double bond equivalent (DBE), oxidation state of carbon atoms (OS_C), modified aromaticity index (AI_{mod}), and the effective number of oxygen atoms ($O_{\rm eff}$) were calculated for the obtained molecular formulas. The DBE, which quantifies the number of rings and double bonds in a molecule (Koch and Dittmar, 2006), was calculated using Eq. (2):

$$DBE = \frac{2 \times c + 2 - h + n}{2} \tag{2}$$

The OS_C was estimated according to Eq. (3) described by Kroll et al. (2011):

$$OS_C \approx 2 \times o/c - h/c \tag{3}$$

The AI_{mod} was first proposed by Koch and Dittmar (2006, 2016) to evaluate the aromaticity of compounds identified through high-resolution mass spectrometry. The index is calculated based on two parameters. DBE_{AI} is the DBE of molecular core structure, and C_{AI} is the number of carbon atoms in the core structure. AI_{mod} is defined as the DBE_{AI} to C_{AI} ratio, with the $AI_{mod} = 0$ when either $DBE_{AI} \le 0$ or $C_{AI} \le 0$ (Brege et al., 2018):

$${\rm AI_{mod}} = \frac{{\rm DBE_{AI}}}{C_{\rm AI}} = \frac{1 + c - 0.5 \times o - s - 0.5 \times (h + n)}{c - 0.5 \times o - s - n} \eqno(4)$$

The O_{eff} was evaluated following Eq. (5):

$$O_{\text{eff}} = o - 2 \times n - 3 \times s \tag{5}$$

In the aforementioned formulas, c, h, o, n, and s represent the number of C, H, O, N, and S atoms, respectively, in the molecular formulas of the corresponding compounds. The ratios DBE/C and $O_{\rm eff}/C$ indicate the degree of aromaticity and oxidation of compounds, respectively.

An intensity-weighted parameter (P_w) for CHOX compounds was calculated using Eq. (6):

$$P_{\rm W} = \sum (P_i \times I_i) / \sum I_i \tag{6}$$

where P represents the following parameters: DBE, DBE/C, O_{eff}/C , OSc, or AI_{mod} . P_i corresponds to the specific parameter value for individual compound i and I_i denotes the signal intensity of compound i. The weighted parameters for both sampling sites are summarized in Table S2.

3 Results and Discussion

3.1 Overview of the sampling period

During the sampling period, distinct differences in conventional air pollutants were observed between the urban and seaside sites. As shown in Table S1, primary-emitted and

traffic-related pollutants like CO and NO_x exhibited significantly higher concentrations at the urban site compared to the seaside site, while an opposite trend was observed for SO₂ concentrations (t test, p < 0.001). Additionally, the seaside site displayed enhanced O₃ concentrations and UVB intensity, indicating more favorable conditions for photochemical reactions. The average OC/EC ratio in PM_{2.5} was 6.7 ± 4.4 at the seaside site, significantly higher than the urban site value of 4.0 ± 0.8 (t test, p < 0.001). Both sites exceeded the SOA formation indicator value (OC/EC = 2) proposed by Chow et al. (1996), indicating strong SOA production in the study area, particularly at the seaside site. In this study, a total of 737 and 768 organic molecules (CHOX) were identified by FIGAERO-I-CIMS for the urban site and the seaside site, respectively. Significant correlations were observed between CHOX signal intensities and OC concentrations at both sites (R = 0.70 and 0.80, Fig. S3), demonstrating the reliability of the OA molecule detection method in this study. The number of identified molecules is comparable to that at a rural site in Southeast US (769 organic molecules, Chen et al., 2020) but lower than those observed in highly industrialized urban areas such as Beijing (939 molecules, Cai et al., 2022) and Guangzhou (815 molecules, Ye et al., 2021). These spatial differences highlight the significant influence of environmental conditions on OA molecular composition.

As described in the methodology section, the identified CHOX were classified into four groups. CHO and CHON compounds were predominant in quantity (Fig. 1a), accounting for 46% and 47% of the total CHOX at the urban site, and 38% and 42% at the seaside site, respectively. In terms of signal intensity, CHO and CHON contributed over 70 % and 20 % to the total CHOX, respectively, at both sites (Fig. 1b). This observation is consistent with the welldocumented predominance of CHO compounds across various environments, including urban areas (e.g., $65 \pm 5 \%$ in Beijing) (Cai et al., 2022), rural areas (79.9 \pm 5.2 % on average in the Rhine river valley, Hyytiälä boreal forest, Finland, and Alabama, US; 87.7±10.8 % in Georgia, US) (Chen et al., 2020; Lopez-Hilfiker et al., 2016) and mountain sites (e.g., $66.2 \pm 5.5 \%$ in Chacaltaya, Bolivia) (Bianchi et al., 2022). In addition, enhanced contributions of CHON compounds are consistently found at the urban sites, such as in Beijing $(30 \pm 5\%)$ (Cai et al., 2022) and on average across Stuttgart and Karlsruhe, Germany and Delhi, India $(27.1 \pm 4.3 \%)$ (Haslett et al., 2023; Huang et al., 2019, 2024), strongly suggesting an association with urban NO_x enrichment.

The molecular masses were identified within the range of m/z 200–500 (Fig. S4). The highest relative abundances, covering m/z 200–320, were found for CHO compounds, while CHON was mainly concentrated in the range of m/z 320–400. These characteristics are consistent with the results reported from Beijing, Wuhan, and Xi'an (Cai et al., 2022; Xin et al., 2024; Shang et al., 2024). As shown in Figs. 1d and S5, the signal intensities of CHO and CHON were steadily higher at the urban site, whereas the signals of

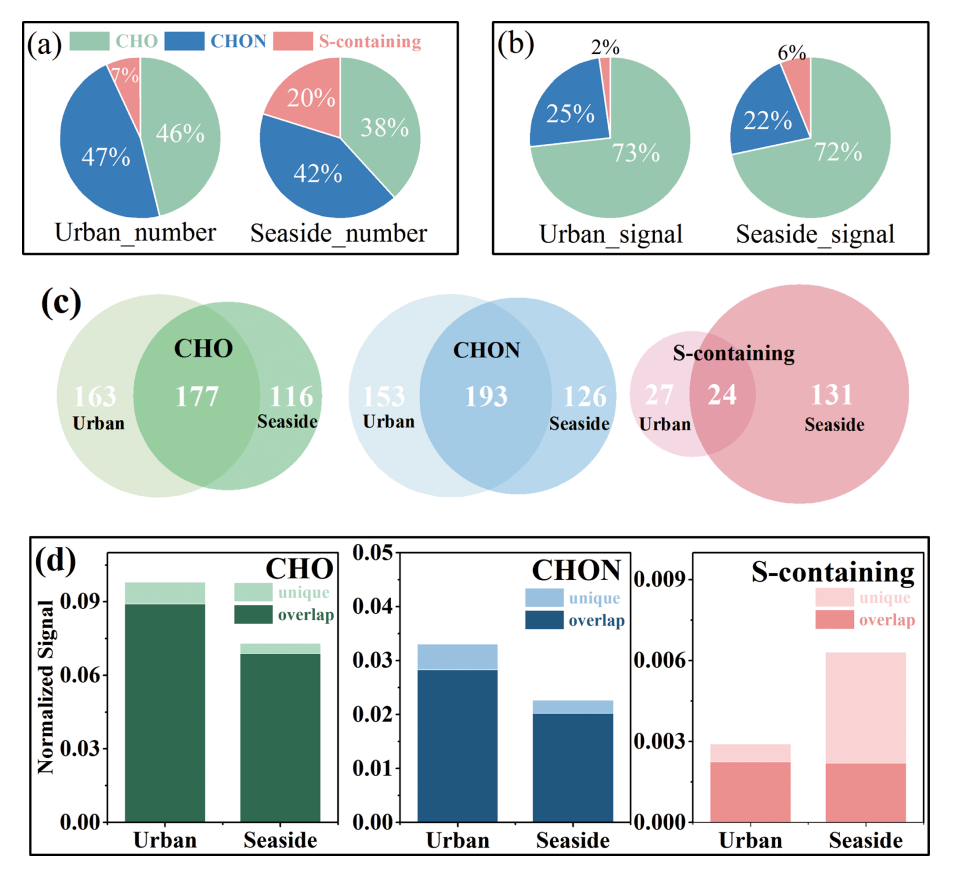


Figure 1. Numbers (**a**) and signals intensity (**b**) proportion of CHO, CHON, and S-containing compounds in CHOX, Venn diagram of the number distribution of overlapping molecular formulas between sites (**c**), and average signals of overlapping and unique CHO, CHON, and S-containing compounds at both sites (**d**).

S-containing compounds were more pronounced at the seaside site. These differences align with the elevated NO₂ at the urban location and the higher SO₂ measured at the seaside location during sampling (Table S1). Comparing CHOX chemical compounds at the two sites (Figs. 1c and S6), we found that over 50% of CHO and CHON molecules at both sites shared the same molecular formula, accounting for 86%–94% of total signals. Notably, the overlapping S-containing compounds constituted only a minor proportion of total S-containing species at the seaside site (35%). These results reveal distinct variations in OA composition between the urban and seaside sites, attributable to differences in anthropogenic emission influences. To further explore the discrepancies in CHOX compounds between the two sites, the characteristics and properties of CHOX were analyzed in detail.

3.2 Characteristics and Properties of CHOX Compounds

3.2.1 The Characteristics of CHOX Distribution

The bulk molecular formulas of CHOX compounds were determined as $C_{10.8}H_{13.7}N_{0.5}O_{5.4}S_{0.1}$ at the urban site

and $C_{10.7}H_{14.4}N_{0.4}O_{5.4}S_{0.2}$ at the seaside site, with mean weighted effective oxygen numbers to carbon content $(O_{\rm eff}/C)$ ratios of 0.82 and 0.85, respectively, indicating the highly oxidized nature of these compounds in the coastal region. In comparison, the bulk CHOX composition at the seaside site exhibited a higher O/C ratio, fewer CHON compounds, and more S-containing compounds. The elevated CHON signal intensity at the urban site could be attributed to the high NO_x concentrations from vehicle emissions, facilitating nitrogen-containing compound formation. In contrast, the enhanced S-containing compound signals at the seaside site likely resulted from marine-driven sources.

Figures 2 and S7 show the signal intensity and quantity distribution of CHO and CHON compounds as a function of carbon number. The distribution characteristics of CHO and CHON compounds were broadly consistent between the two sites. As shown in Fig. S7, the quantity of CHO compounds exhibited a normal distribution with carbon number, mainly concentrated in the ranges of 8–14 carbon and 4–6 oxygens, while the distribution of CHON compounds was relatively uniform, with a minor abundance peak at C_{6-10} and O_{5-6} . In contrast to the quantity distribution, the signal intensity of CHO compounds decreased with increasing

carbon number (Fig. 2a-b). Both sites exhibited significant signal contributions from O₄-CHO compounds, which likely correspond to dicarboxylic acid species. Oxalic acid (C₂) and succinic acid (C₄) were the most abundant species, followed by malonic acid (C₃). These low-molecular-weight dicarboxylic acids are typically associated with aqueous reactions (Lim et al., 2010). With increasing carbon number, the dominant oxygen content in CHO compounds shifted from O_4 to O_{5-6} . The signals of CHON compounds were predominantly concentrated in the C_{3-10} range, with their oxygen content shifting from O₃ to O₅₋₇ as carbon number increased (Fig. 2c-d). Site-specific differences in molecular distribution were observed. CHO and CHON compounds with high carbon content (> C₁₀) exhibited stronger signal intensities at the urban site than the seaside site, with O₆-CHO and O₇₋₈-CHON species showing particular enhancement. As shown in Figs. S8 and S9, the proportion of O₆-CHO species increased significantly with carbon number at the urban site, reaching up to 41 % and 61 % at C_{14-15} . These likely correspond to molecular formulas such as C₁₄H₁₆O₆ and C₁₅H₁₈O₆, which are oxidation products of sesquiterpenes. Under the combined influence of anthropogenic and biologic emissions, OA compounds at both sites included products from photochemical oxidation of aromatic VOCs and oxidation of biological precursors such as isoprene and monoterpenes. However, composition differed between sites, with the urban site showing higher signal intensity of species including $C_3H_4O_4$, $C_{5-6}H_4O_5$, $C_{8-9}H_{12}O_4$, and $C_6H_{11}NO_6$, while the seaside site exhibited stronger signal intensity of species such as $C_{9-10}H_{16}O_3$, $C_4H_{4/6}O_5$, $C_5H_8O_4$, and $C_9H_{15}NO_5$.

3.2.2 The Unsaturation, Oxidation State, and Aromaticity of CHOX Compounds

The double bond equivalent (DBE) characterizes the potential number of rings and double bonds in organic compound molecules. Quantitatively, CHOX compounds were predominantly distributed within the DBE range of 2–8 (Fig. S10). In terms of signal intensity (Fig. 3), CHO compounds exhibited significant contributions in the DBE = 2-4 range, while CHON compounds were concentrated in the DBE = 2-5range. Compounds with DBE \geq 6 showed higher signal contributions at the urban site (9%) than at the seaside site (7%). These highly unsaturated compounds may undergo oxidative transformation into higher molecular weight products, being particularly prone to photooxidation with oxidants like O₃ to form C=O bonds in carbonyls and carboxylic acids (Zhao et al., 2014). As shown in Table S2, the weighted-DBE values of CHOX compounds ranged from 2.32 to 3.68, which is close to the previously reported values (2.64-3.82) for urban and marine samples (Xin et al., 2024). The urban site exhibited higher weighted-DBE values for CHOX compounds (3.25) compared to the seaside site (2.99) (Table S2), indicating distinct formation pathways. The highly unsaturated CHOX compounds are likely derived from anthropogenic precursors such as aromatic VOCs and PAHs, whereas the more saturated components primarily originated from biogenic terpene compounds and saturated fatty acids from marine sources (Du et al., 2024; Chan et al., 2011; Nguyen et al., 2012; Noziere et al., 2010).

DBE/C ratios greater than 0.7 generally indicate the presence of soot materials or oxidized polycyclic aromatic hydrocarbons (PAHs) (Cui et al., 2019). During the sampling period, while the signal proportions of compounds with DBE/C > 0.7 were comparable between the two sites (CHO: $\sim 25\%$; CHON: $\sim 16\%$), their number proportions were significantly higher at the urban site (CHO: 17%; CHON: 22%) than at the seaside site (CHO: 6%; CHON: 19%). Consistent with the above discussion, S-containing compounds with DBE/C > 0.7 exhibited higher proportions in both signal intensity and quantity at the urban site (24 % and 26%, respectively) compared to the seaside site (14% and 10%, respectively). The systematically higher DBE/C ratios for OA compounds at the urban site suggest more contribution from soot materials and/or oxidized PAHs, which aligns with the observed EC concentrations (urban: $1.57 \pm$ $0.80 \,\mu g \, m^{-3}$; seaside: $0.91 \pm 0.42 \,\mu g \, m^{-3}$). The AI_{mod}, which reflects the minimum number of carbon-carbon double bonds and aromatic rings (Koch and Dittmar, 2006, 2016), was correspondingly higher at the urban site (weighted- AI_{mod} = 0.17) than at the seaside site (0.15), further supporting the greater contribution of aromatic species to urban OA.

The carbon oxidation state (OSc), a parameter introduced by Kroll et al. (2011), serves to quantify the oxidation degree of organic mixtures undergoing dynamic atmospheric processes. The weighted-OSc values of CHOX compounds were higher at the seaside site (0.55) than at the urban site (0.49) (Table S2), consistent with the aforementioned enhanced SOA formation at the seaside site. The van Krevelen (VK) diagrams (Fig. S11) revealed that homologue series such as $C_n H_{2n-x} O_4$ (where x = 2, 4, 6) made significant contributions to CHOX compounds in this study. The elevated weighted-OSc values of seaside CHO compounds could be attributed to the strong signal intensities of low-carbon-number homologues, such as $C_nH_{2n-2}O_4$ and $C_nH_{2n-4}O_4$. In contrast to CHO compounds, both CHON and S-containing compounds exhibited higher weighted-OSc values at the urban site, indicating a more chemically aged state of N- and S-containing species. The increased weighted-OSc of urban CHON compounds mainly resulted from enhanced signals of highly oxidized species, such as C₃H₅NO₆ and C₅H₇NO₆. These compounds are likely formed through multi-generational oxidation of aromatic or biogenic VOCs, ultimately yielding products containing highly oxidized functional groups, such as -COOH and -ONO2. The relatively low weighted-OSc of seaside S-containing compounds was likely associated with fresh sulfur emissions from local sources, including oceanic discharge and ship exhaust. Furthermore, S-containing compounds in seaside OA contained more Aliphatic-like OSs

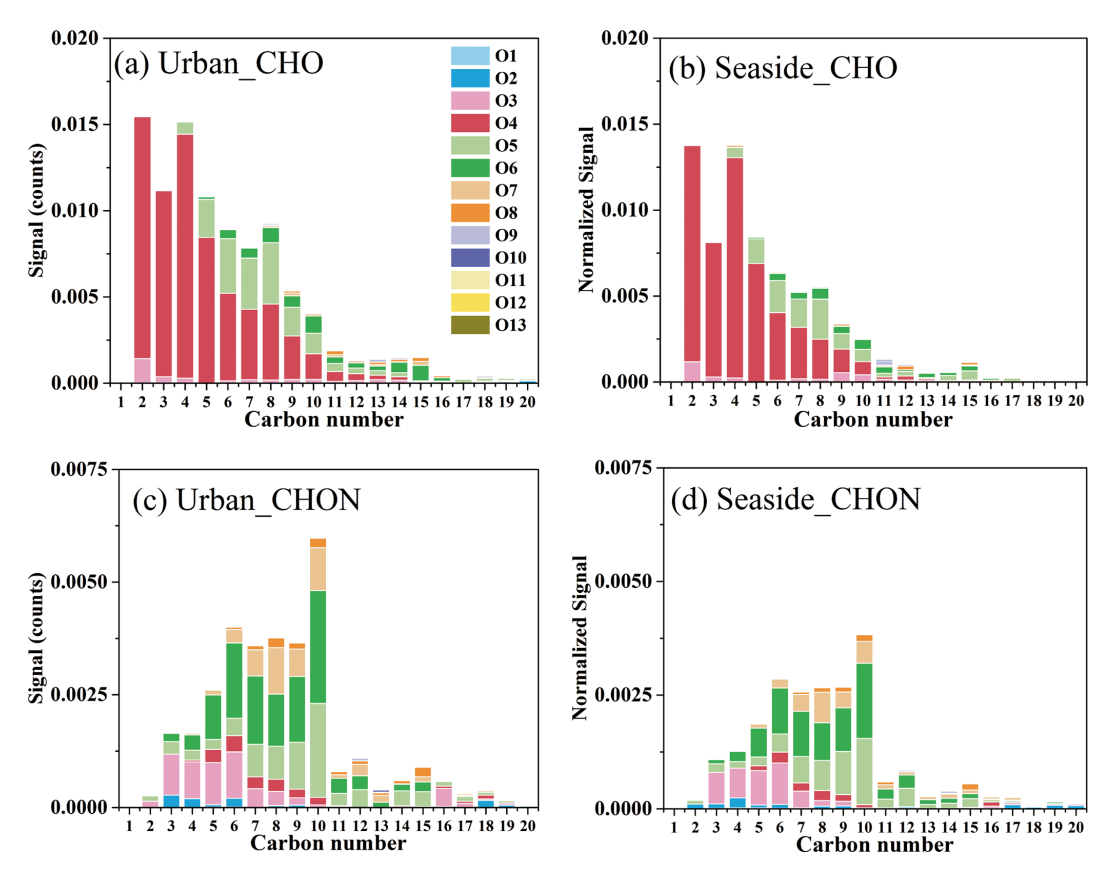


Figure 2. Signal intensity of CHO and CHON categorized by the number of carbon atoms at the urban (a, c) and seaside (b, d) sites.

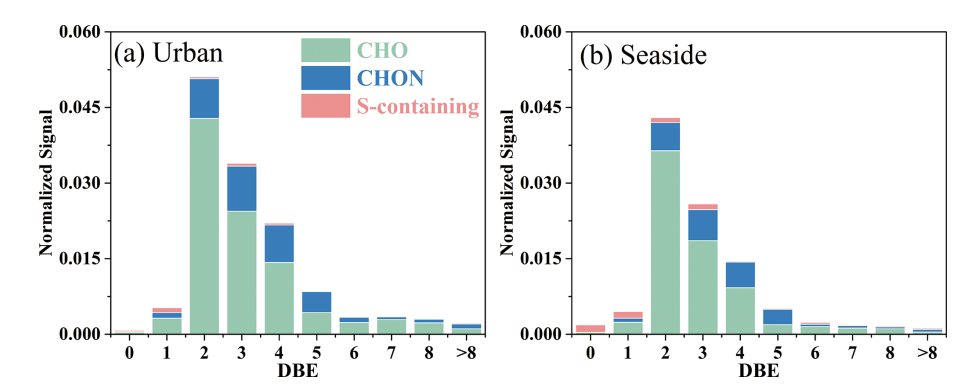


Figure 3. Signal intensity of CHOX categorized by double bonds equivalent (DBE) at the urban site (a) and the seaside site (b).

species with low carbon numbers, such as $C_nH_{2n/2n+2}O_{4-5}S$ (n=2-4), and Reduced-sulfur species (O < 4) (to be discussed later), which also contributes to their relatively low weighted-OSc values. This observation is consistent with previous findings that S-containing compounds in primary organic sea spray aerosols were predominantly composed of fatty acids and other lipid molecules with lower oxidation degrees (Siegel et al., 2021). Additionally, the limited number of identified S-containing compounds may have artificially inflated the weighted-OSc values for urban S-containing compounds.

3.2.3 The Classification of CHOX Compounds

As shown in Fig. 4, CHOX compounds were categorized based on AI_{mod} , DBE, H/C, and O/C ratios. Low H/C ratios, combined with high DBE and AI_{mod} values indicate a high degree of unsaturation and the presence of aromatic structures. CHOX were classified into Aromatic-like and Aliphatic-like compounds based on AI_{mod} and H/C, following the methodology of Xin et al. (2024). Compounds with $AI_{mod} > 0.5$ or $AI_{mod} \le 0.5$ and H/C < 1.5 were defined as Aromatic-like compounds. Conversely, compounds

with $AI_{mod} \leq 0.5$ and $H/C \geq 1.5$ were defined as Aliphatic-like compounds (Coward et al., 2019). The categorical distribution of CHOX compounds showed similarities between the two sites, with Aromatic-like CHOX species contributing significantly to the signal at both sites (> 50 %). Nevertheless, their relative abundance was markedly higher at the urban site, while the seaside site exhibited a greater proportion of Aliphatic-like compounds (42.0 % vs. 39.2 %).

Using an O/C threshold of 0.5, both Aromatic-like and Aliphatic-like CHOX were further subdivided into two subcategories, with O-rich (O/C > 0.5) compounds being more abundant than O-poor (O/C < 0.5) compounds. The signal ratios of O-rich to O-poor compounds were higher at the seaside site for both categories. Specifically, the O-rich / O-poor ratio for Aromatic-like CHOX was 4.9 at the seaside site versus 4.1 at the urban site. Similarly, the ratio for Aliphaticlike CHOX was 3.9 at the seaside site compared to 3.3 at the urban site. These results are consistent with the findings of OC/EC ratios and OSc discussed earlier, suggesting that the seaside atmosphere is more conducive to the formation of highly oxidized organic compounds. Notably, the proportion of Aliphatic-like O-rich CHOX was significantly higher at the seaside site than at the urban site, aligning with a recent study that reported elevated levels of Aliphatic-like O-rich CHOX in marine-remote PM_{2.5} (Xin et al., 2024). This finding demonstrates a consistent spatial pattern that urban OA is more strongly influenced by anthropogenic emissions and is dominated by aromatic species, whereas marine-influenced OA exhibits relatively higher proportions of aged, aliphatic compounds.

For CHON compounds, Aromatic-like compounds with $O/N \ge 2$ and Aliphatic-like compounds with $O/N \ge 3$ were categorized as Nitro-aromatic compounds (NACs) and Aliphatic Nitrates, respectively, while the remaining compounds were classified as Reduced-nitrogen compounds. The distribution patterns of CHON classifications were highly consistent between the two sites. Aliphatic-like CHON exhibited the highest signal proportion, followed by NACs, with Reduced-nitrogen compounds showing the lowest signal contribution. The most abundant compound in Aliphaticlike CHON was C₁₀H₁₅NO₆, accounting for 7.5 % of total signals at both sites. Previous studies have demonstrated that C₁₀H₁₅NO₆ is produced through nitrate radical (NO₃•)initiated oxidation of monoterpenes (e.g., limonene or β pinene, C₁₀H₁₆) (Boyd et al., 2015; Faxon et al., 2018). The signal profiles of NACs were dominated by $C_nH_{2n-7}O_xN$ homologues (e.g., C₆H₅NO₃ and C₇H₇NO₃) at both sites. Their prevalent presence is primarily attributable to formation pathways initiated by the oxidation of VOCs under anthropogenic influence, coupled with elevated NO_x levels (Wang et al., 2019; Xia et al., 2023; Xie et al., 2017). While biomass burning emissions were relatively limited in the study area, NACs and their aromatic VOC precursors likely originated from other combustion sources, such as coal combustion, traffic emissions, and industrial activities (Lu et al., 2019a, b, 2021). Notably, NACs with DBE \geq 6 exhibited higher signal intensities at the urban site, suggesting a stronger contribution from these combustion emissions.

Following Lin et al. (2012) and Xie et al. (2020), S-containing compounds with $O/S \ge 4$ were defined as organosulfates (OSs) and further divided into three subcategories: (1) Aromatic-like OSs (AI_{mod} > 0.5, or AI_{mod} \leq 0.5 with H/C < 1.5); (2) Aliphatic-like OSs (AI_{mod} \leq 0.5, H/C \geq 1.5, and DBE \leq 2); (3) Biogenic-like OSs $(AI_{mod} \le 0.5, H/C \ge 1.5, and DBE > 2)$. Compounds with O/S < 4 were classified as Reduced-sulfur compounds. Unlike CHO and CHON, the classification distribution of Scontaining compounds differed significantly between the two sites. At the urban site, the signal profiles were dominated by Aromatic-like OSs, followed by Aliphatic-like OSs. In contrast, the seaside site exhibited the highest signal proportion of Aliphatic-like OSs, primarily contributed by $C_3H_6O_5S$, $C_3H_8O_5S$, and $C_4H_{10}O_5S$. Additionally, the seaside site showed higher signal intensities of Reducedsulfur compounds, largely due to abundant $C_nH_{2n-4}O_xS$ and $C_nH_{2n+2}O_xS$ homologues. The elevated abundances of Aliphatic-like OSs and Reduced-sulfur compounds in seaside OA were likely attributed to the oxidation of biogenic reduced sulfur gases, particularly dimethyl sulfide (DMS) emitted from the ocean (Shen et al., 2022; Siegel et al., 2021).

3.3 Case study: Evolution of molecular compositions

To investigate the impact of atmospheric processes on organic molecular composition, we selected two distinct episodes with significant increases in PM_{2.5} concentrations (Case 1: 26-29 March; Case 2: 10-13 April) for further analysis (Fig. S12). In Case 1, the daily average offline PM_{2.5} concentration increased from 27.35 to $38.80 \,\mu g \,m^{-3}$ at the urban site and from 27.37 to $45.89 \, \mu g \, m^{-3}$ at the seaside site. While in Case 2, it increased from 17.13 to $59.78 \,\mathrm{ug}\,\mathrm{m}^{-3}$ at the urban site and from 17.11 to $40.63 \,\mu\mathrm{g}\,\mathrm{m}^{-3}$ at the seaside site. Backward trajectory analysis (Fig. S13) revealed that the air masses in Case 1 were transported from North China along the coastline to study area over a long distance and then shifted to local air masses. This transport pattern was accompanied by initially elevated nighttime O₃ concentrations under regional influence, followed by a significant rise in NO_x levels due to local accumulation. RH in Case 1 remained relatively stable at both sites, averaging approximately 72 % (urban) and 86 % (seaside). In contrast, the air masses in Case 2 were primarily influenced by long-range marine transport. The O_x levels displayed repetitive and stable diurnal variations. Notably, RH progressively increased from 66 % to 91 % at the urban site and from 76 % to 99 % at the seaside site, while UVB intensity declined gradually from 12.6 to $5.4\,\mathrm{W\,m^{-2}}$ at the urban site and from 12.4 to $8.7 \,\mathrm{W}\,\mathrm{m}^{-2}$ at the seaside site. We also observed that as Case 2 progressed, the NO_3^- and SO_4^{2-} concentrations increased

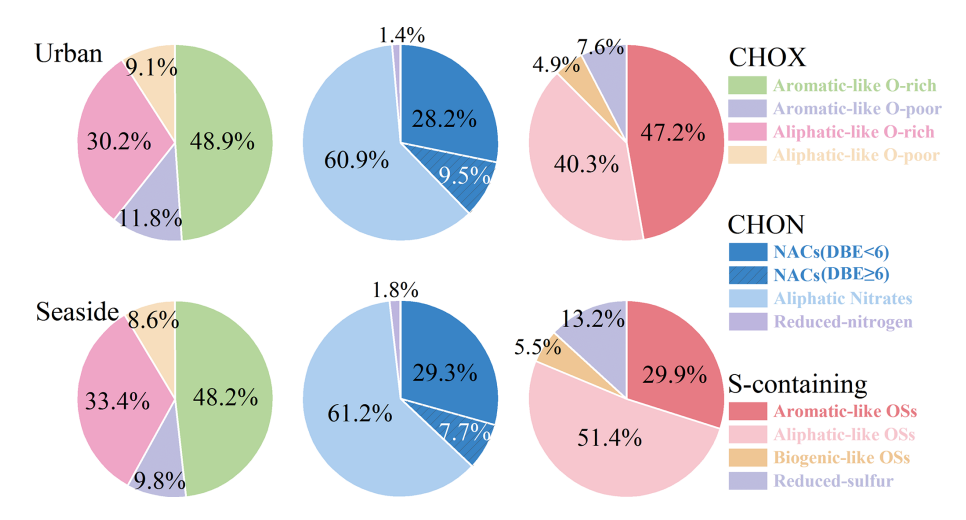


Figure 4. Fraction of CHOX signal intensity categorized by different parameter.

markedly with rising RH. Overall, the two episodes exhibited distinct source origins and environmental conditions.

The evolution of daily CHOX signal intensity during pollution episodes is presented in Fig. 5. Case 1 exhibited higher CHOX signal intensities than Case 2. Spatially, the urban site showed higher levels of CHO and CHON compounds, while the seaside site had relatively higher concentrations of S-containing compounds, consistent with the general characteristics of the two sites. During Case 1, all CHOX compounds showed increased signal intensities, particularly urban CHON and seaside S-containing compounds (Fig. 5b-d). This feature aligns with the earlier hypothesis that local emissions dominantly contributed to CHOX in this episode. As expected, NO_x concentrations were significantly higher at the urban site $(38.21 \, \mu \mathrm{g \, m}^{-3})$ than at the seaside site $(24.91 \,\mu\text{g m}^{-3})$, while SO₂ levels exhibited an inverse trend (urban: $3.29 \,\mu\mathrm{g}\,\mathrm{m}^{-3}$; seaside: $4.54 \,\mu\mathrm{g}\,\mathrm{m}^{-3}$). In contrast, Case 2 (Fig. 5b-d) was characterized by a significant temporal increase in CHO compounds, while CHON levels remained stable. Additionally, S-containing compounds showed a slight but synchronized enhancement at both sites, likely due to the influence of a common marine air mass source. Given the more pronounced variations in CHOX composition at the urban site, we conducted further analysis on CHOX at this location.

Figure 6 illustrates the compositional changes of CHOX compounds during the two pollution episodes. The OSc (0.37) of CHOX in Case 1 was significantly lower than the campaign average (0.49). Regarding CHOX composition, as the dominant influence shifted from long-distance transport to local accumulation, the proportion of Aliphatic-like Orich components in CHOX decreased, while Aliphatic-like Opoor components contributed increasingly. These observations reflect the enhanced influence from local anthropogenic emissions. Our aforementioned results have shown a significant enhancement of CHON signals in Case 1. Further com-

positional analysis revealed that as the episode progressed, the proportion of NACs (DBE < 6) in CHON compounds decreased, while the proportion of Aliphatic Nitrates increased. Figure 7a-d specifically show that the urban CHON signal enhancement was primarily driven by low DBE/C compounds, including C₁₀H₁₉NO₅, C₁₀H₁₅NO₆, C₄H₇NO₃, C₆H₁₁NO₆, and C₃H₇NO₃. These organonitrates are mainly formed through the oxidation of VOCs such as alkanes, alkenes and monoterpenes by OH, O₃, and NO₃ in the presence of NO_x (Lee et al., 2016; Ng et al., 2017; Yan et al., 2016; Yang et al., 2025), and subsequently partition into the particle phase. Additionally, particulate organonitrates can also be generated via heterogeneous reactions of organic compounds with NO₃ (Nah et al., 2016). During Case 1, elevated O₃ concentrations resulting from regional transport (Fig. S12a) likely facilitated nocturnal NO₃ radical formation (via NO₂+O₃). Online CIMS measurements also revealed that N₂O₅ signals in Case 1 were one order of magnitude higher than in Case 2 (data not shown). Hence, nocturnal oxidation of monoterpenes by NO₃, yielding products such as C₁₀H₁₉NO₅ and C₁₀H₁₅NO₆, might have led to the observed increase in the proportion of Aliphatic Nitrates.

Case 2 exhibited different characteristics compared to Case 1 (Fig. 6). The OSc (0.51) of CHOX compounds in Case 2 increased in contrast to the campaign average (0.49). The proportion of Aliphatic-like O-rich compounds demonstrated a continuous upward trend, rising from 28 % to 39 % at the urban site, while Aromatic-like O-rich compounds remained stable. Conversely, the proportion of both Aromatic-like O-poor and Aliphatic-like O-poor compounds decreased. The overall increase in OSc and the high abundance of Aliphatic-like O-rich compounds can be attributed to the influence of marine air masses. Although these air masses diluted OA concentrations, they introduced aliphatic compounds and enhanced atmospheric oxidative capacity likely via abundant halogen radicals, thereby driving the ob-

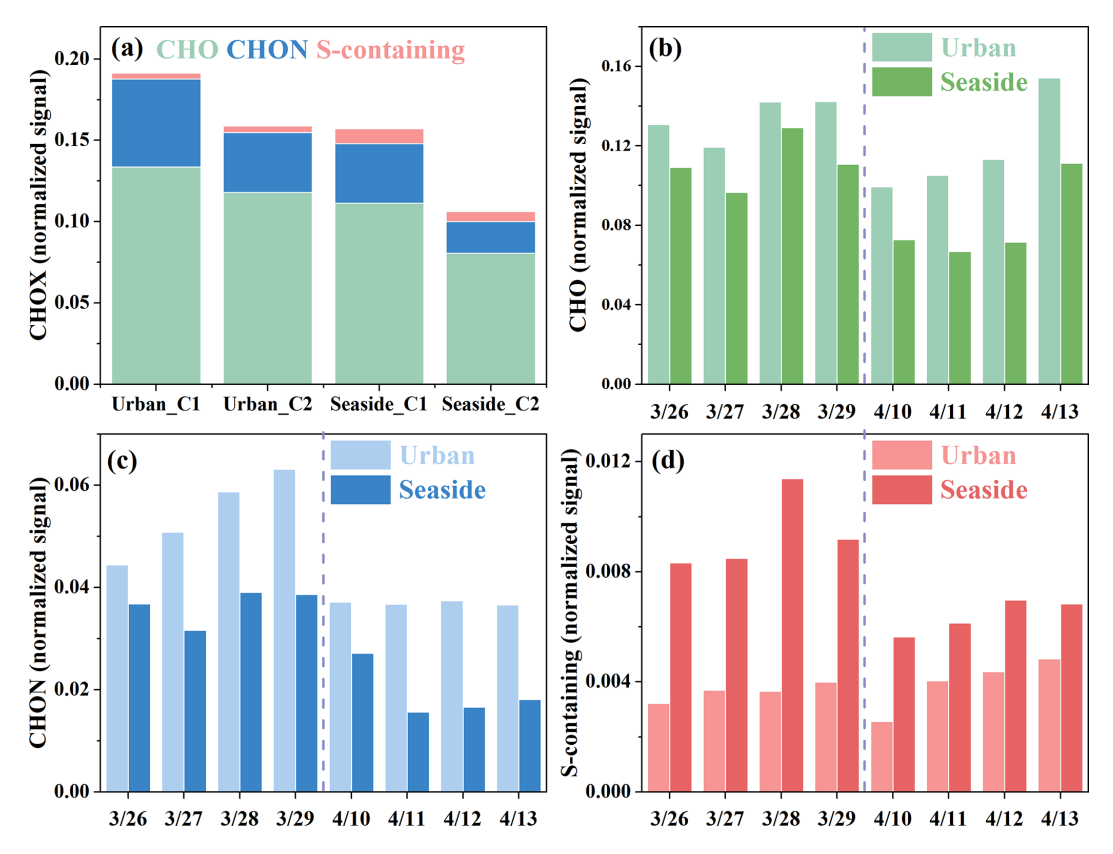


Figure 5. Signal intensity of CHOX during the different periods at the two sites.

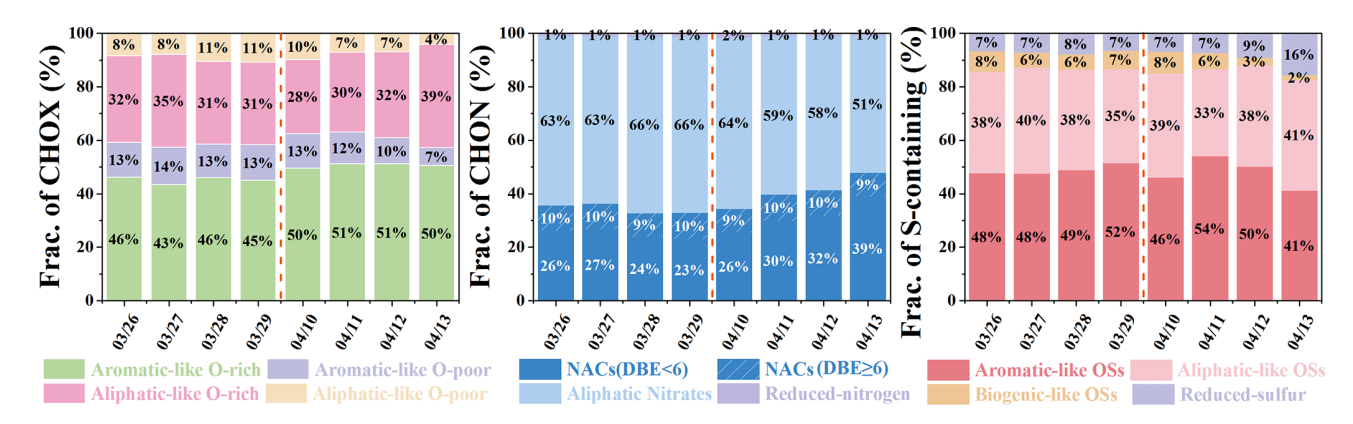


Figure 6. Fraction distribution of urban CHOX signal intensity categorized by different parameter (AI $_{mod}$, DBE, H/C, and O/C) during Case 1 and Case 2.

served changes. Unlike CHO compounds, the total signal intensities of CHON compounds in Case 2 remained relatively constant (Fig. 5c), but their molecular composition underwent significant changes. Specifically, the proportion of NACs (DBE < 6) in CHON compounds increased from 26% to 39% at the urban site, whereas Aliphatic Nitrates decreased correspondingly from 64% to 51%. The variation of CHON compositions indicates a change in the formation pathways of N-containing compounds. The notably higher RH in Case 2 would facilitate the uptake of gas-phase

NACs into aerosols (Frka et al., 2016; Vidovic et al., 2018) and probably their heterogeneous reactions with NO₃ radicals. Concurrently, reduced UVB diminished the photolytic degradation of NACs (Peng et al., 2023). This dual effect collectively led to the observed increase in the proportion of NACs. Additionally, variations in S-containing compounds were generally consistent across both sites (Fig. S14), with the most notable increases observed in Aliphatic-like OSs and Reduced sulfur compounds.

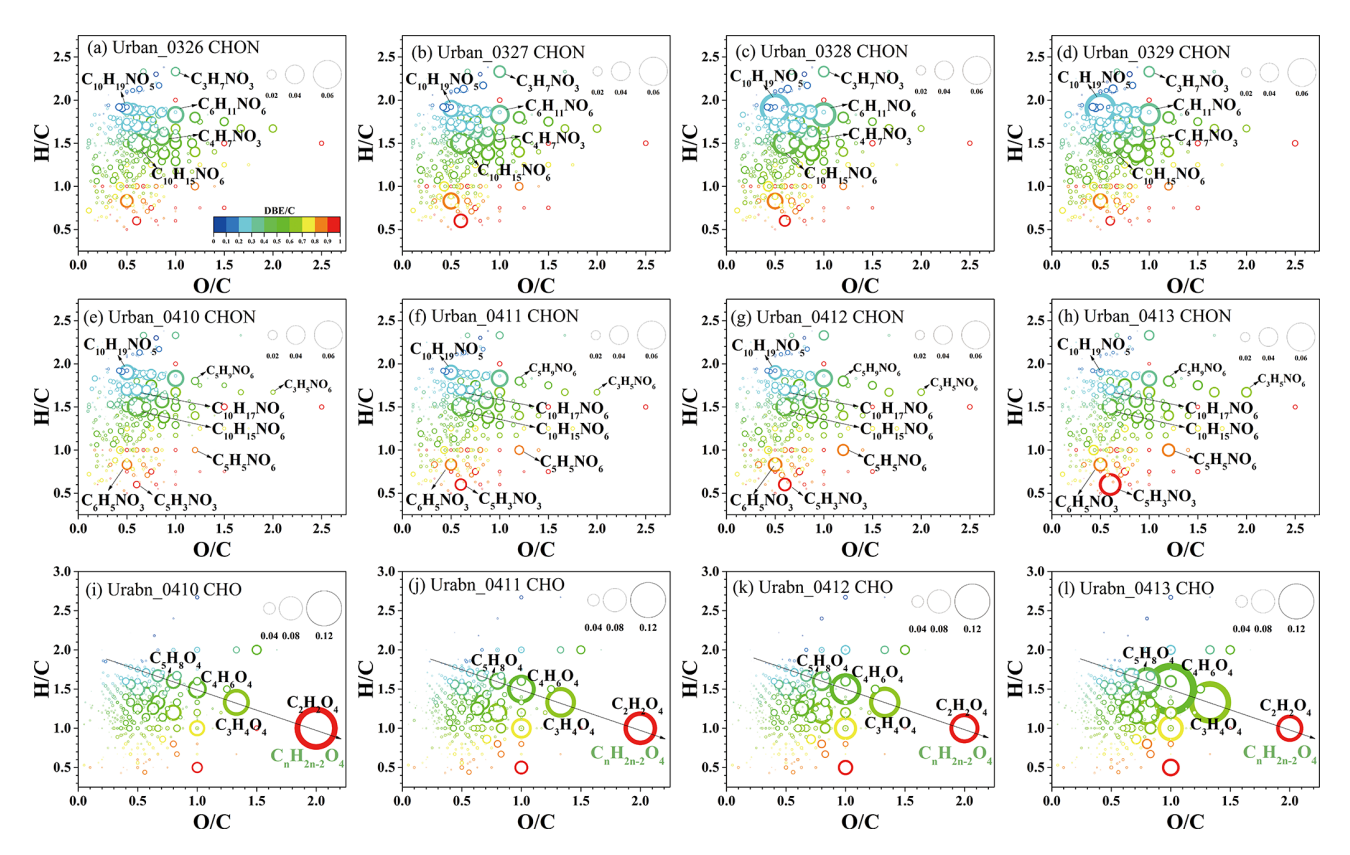


Figure 7. The van Krevelen (VK) diagram of urban CHON (a-h) and CHO (i-l) day by day during different periods. The circle size corresponds to signal intensity and the color scale represents the DBE/C ratio.

A distinct characteristic of Case 2 was the increased signal intensity of CHO compounds (Fig. 5b), particularly on 13 April. The VK diagrams (Fig. 7i-1) showed that CHO compounds evolved into highly oxidized species (e.g., C₂H₂O₄, C₄H₆O₄, C₅H₈O₄) as aerosol concentrations increased. Previous studies have demonstrated that organic acids are continuously generated during aqueous photochemical aging processes (Ervens et al., 2011; Ye et al., 2025). The $C_nH_{2n-2}O_4$ homologues, such as $C_4H_6O_4$ (succinic acid) and C₃H₄O₄ (malonic acid), were predominantly formed via aqueous-phase reactions and/or photochemical oxidation of VOCs (Kawamura and Bikkina, 2016). The C₅H₈O₄ species likely represents glutaric acid, a known oxidation product of isoprene (Berndt et al., 2019). Research indicates that aqueous-phase reactions play a crucial role in generating highly oxidized OA (Xu et al., 2017b). We therefore infer that the increased RH under marine air mass influence during Case 2 promoted aqueous reaction-driven organic aerosol formation, thereby enhancing OA oxidation levels. This interpretation is supported by the observation that CHO compounds at the seaside site exhibited higher oxidation degrees than those at the urban site (Table S2). Regarding CHON compositional changes, the VK diagrams clearly showed a decline in signals from low DBE/C species (e.g., $C_{10}H_{19}NO_5$, $C_{10}H_{15}NO_6$, and $C_{10}H_{17}NO_6$) alongside an increase in oxygen-rich and lower-carbon species (e.g., $C_6H_5NO_3$, $C_5H_3NO_3$, $C_3H_5NO_6$, $C_5H_5NO_6$, and $C_5H_9NO_6$, Fig. 7e–h). These CHON compounds most likely originated from aromatic hydrocarbon oxidation followed by atmospheric aging processes, leading to concurrent increases in both weighted-AI_{mod} (0.16 vs. 0.14) and weighted-OSc (0.02 vs. -0.08). Overall, the compositional evolution in Case 2 demonstrates that marine-derived humid air masses enhanced aqueous-phase reactions, thereby promoting organic aerosol formation and intensifying oxidative states.

4 Conclusions

This study investigates the molecular characteristics and chemical evolution of OA in coastal environments (urban and seaside sites) through FIGAERO-I-CIMS analysis of $PM_{2.5}$ samples collected during spring 2024. CHO and CHON compounds dominated the OA composition at both sites, sharing over 50 % of molecular formulas and accounting for 86 %–94 % of total signal intensities. The urban site exhibited higher signal intensities of CHON compounds, while the seaside site showed elevated S-containing compounds. These results clearly reflect distinct source-specific molecular fingerprints. The $O_{\rm eff}/C$ values (urban 0.82; seaside 0.85) indicated the highly oxidized nature of coastal compounds. Com-

pared to urban OA, Seaside OA exhibited lower unsaturation, reduced aromaticity, and higher oxidation states. Categorization showed that Aromatic-like CHOX exhibited higher signals than Aliphatic-like compounds at both sites, while urban OA was enriched in aromatic species (e.g., NACs from vehicle- and combustion-related emissions) and seaside OA featured aliphatic and highly oxidized compounds. Two pollution episodes were selected to investigate CHOX evolution mechanisms. Case 1 (local accumulation) exhibited a significant increase in urban CHON compounds, likely attributable to elevated NO_x levels that promoted the formation of organonitrates. Case 2 (marine air masses) was characterized by high-humidity conditions that enhanced aqueous-/heterogeneous-phase reactions, thereby promoting the formation of CHO and NACs compounds and intensifying the overall oxidation state. The offline FIGAERO-I-CIMS proved robust for molecular-level characterization of OA across diverse environments. These findings not only advance our understanding of OA molecular characteristics and chemical evolution processes, but also provide insights for region-specific control strategies.

Data availability. The data related to this article are accessible at figshare (https://doi.org/10.6084/m9.figshare.28956629.v1, Chen, 2025).

Supplement. The supplement related to this article is available online at https://doi.org/10.5194/acp-25-16315-2025-supplement.

Author contributions. YC conducted the laboratory experiments. YC and LX analyzed the data and wrote the paper. ZL, CY, GC, RZ, and YZ coordinated the measurements and maintained data. LX, XF, and JC designed the project. JC, YH, and ML supervised the study. All the co-authors contributed to the discussion and commented on the manuscript.

Competing interests. The contact author has declared that none of the authors has any competing interests.

Disclaimer. Publisher's note: Copernicus Publications remains neutral with regard to jurisdictional claims made in the text, published maps, institutional affiliations, or any other geographical representation in this paper. While Copernicus Publications makes every effort to include appropriate place names, the final responsibility lies with the authors. Views expressed in the text are those of the authors and do not necessarily reflect the views of the publisher.

Acknowledgements. The authors acknowledge the National Natural Science Foundation of China, the Science and Technology Department of Fujian Province, State Key Laboratory of Advanced Environmental Technology, the Xiamen Atmospheric Environment

Observation and Research Station of Fujian Province, and the Fujian Key Laboratory of Atmospheric Ozone Pollution Prevention (Institute of Urban Environment, Chinese Academy of Sciences).

Financial support. This research has been supported by the National Natural Science Foundation of China (grant no. U22A20578 and 42277091), the National Key Research and Development Program (grant no. 2022YFC3700304), the Science and Technology Department of Fujian Province (grant no. 2022L3025), the guiding project of seizing the commanding heights of "self-purifying city" (grant no. IUE-CERAE-202402), STS Plan Supporting Project of the Chinese Academy of Sciences in Fujian Province (grant no. 2023T3013), and Xiamen Atmospheric Environment Observation and Research Station of Fujian Province.

Review statement. This paper was edited by Quanfu He and reviewed by three anonymous referees.

References

An, Y., Xu, J., Feng, L., Zhang, X., Liu, Y., Kang, S., Jiang, B., and Liao, Y.: Molecular characterization of organic aerosol in the Himalayas: insight from ultra-high-resolution mass spectrometry, Atmos. Chem. Phys., 19, 1115–1128, https://doi.org/10.5194/acp-19-1115-2019, 2019.

Berndt, T., Hyttinen, N., Herrmann, H., and Hansel A.: First oxidation products from the reaction of hydroxyl radicals with isoprene for pristine environmental conditions, Commun. Chem., 2, 21, https://doi.org/10.1038/s42004-019-0120-9, 2019.

Bianchi, F., Kurten, T., Riva, M., Mohr, C., Rissanen, M., Roldin, P., Berndt, T., Crounse, J., Wennberg, P., Mentel, T., Wildt, J., Junninen, H., Jokinen, T., Kulmala, M., Worsnop, D., Thornton, J., Donahue, N., Kjaergaard, H., and Ehn, M. Highly oxygenated organic molecules (HOM) from gasphase autoxidation involving peroxy radicals: A key contributor to atmospheric aerosol, Chem. Rev., 119, 3472–509, https://doi.org/10.1021/acs.chemrev.8b00395, 2019.

Bianchi, F., Sinclair, V. A., Aliaga, D., Zha, Q., Scholz, W., Wu, C., Heikkinen, L., Modini, R., Partoll, E., Velarde, F., Moreno, I., Gramlich, Y., Huang, W., Leiminger, M., Enroth, J., Peräkylä, O., Marinoni, A., Xuemeng, C., Blacutt, L., Forno, R., Gutierrez, R., Ginot, P., Uzu, G., Facchini, M. C., Gilardoni, S., GyselBeer, M., Cai, R., Petäjä, T., Rinaldi, M., Saathoff, H., Sellegri, K., Worsnop, D., Artaxo, P., Hansel, A., Kulmala, M., Wiedensohler, A., Laj, P., Krejci, R., Carbone, S., Andrade, M., and Mohr, C.: The SALTENA Experiment: Comprehensive Observations of Aerosol Sources, Formation, and Processes in the South American Andes, B. Am. Meteorol. Soc., 103, E212–E229, https://doi.org/10.1175/BAMS-D-20-0187.1, 2022.

Boyd, C. M., Sanchez, J., Xu, L., Eugene, A. J., Nah, T., Tuet, W. Y., Guzman, M. I., and Ng, N. L.: Secondary organic aerosol formation from the β-pinene + NO₃ system: effect of humidity and peroxy radical fate, Atmos. Chem. Phys., 15, 7497–7522, https://doi.org/10.5194/acp-15-7497-2015, 2015.

Brege, M., Paglione, M., Gilardoni, S., Decesari, S., Facchini, M. C., and Mazzoleni, L. R.: Molecular insights on aging

- and aqueous-phase processing from ambient biomass burning emissions-influenced Po Valley fog and aerosol, Atmos. Chem. Phys., 18, 13197–13214, https://doi.org/10.5194/acp-18-13197-2018, 2018.
- Cai, J., Wu, C., Wang, J., Du, W., Zheng, F., Hakala, S., Fan, X., Chu, B., Yao, L., Feng, Z., Liu, Y., Sun, Y., Zheng, J., Yan, C., Bianchi, F., Kulmala, M., Mohr, C., and Daellenbach, K. R.: Influence of organic aerosol molecular composition on particle absorptive properties in autumn Beijing, Atmos. Chem. Phys., 22, 1251–1269, https://doi.org/10.5194/acp-22-1251-2022, 2022.
- Cai, J., Daellenbach, K. R., Wu, C., Zheng, Y., Zheng, F., Du, W., Haslett, S. L., Chen, Q., Kulmala, M., and Mohr, C.: Characterization of offline analysis of particulate matter with FIGAERO-CIMS, Atmos. Meas. Tech., 16, 1147–1165, https://doi.org/10.5194/amt-16-1147-2023, 2023.
- Chan, M. N., Surratt, J. D., Chan, A. W. H., Schilling, K., Offenberg, J. H., Lewandowski, M., Edney, E. O., Kleindienst, T. E., Jaoui, M., Edgerton, E. S., Tanner, R. L., Shaw, S. L., Zheng, M., Knipping, E. M., and Seinfeld, J. H.: Influence of aerosol acidity on the chemical composition of secondary organic aerosol from β-caryophyllene, Atmos. Chem. Phys., 11, 1735–1751, https://doi.org/10.5194/acp-11-1735-2011, 2011.
- Chazeau, B., Temime-Roussel, B., Gille, G., Mesbah, B., D'Anna, B., Wortham, H., and Marchand, N.: Measurement report: Fourteen months of real-time characterisation of the submicronic aerosol and its atmospheric dynamics at the Marseille–Longchamp supersite, Atmos. Chem. Phys., 21, 7293–7319, https://doi.org/10.5194/acp-21-7293-2021, 2021.
- Chen, G., Xu, L., Yu, S., Xue, L., Lin, Z., Yang, C., Ji, X., Fan, X., Tham, Y., Wang, H., Hong, Y., Li, M., Seinfeld, J., and Chen, J.: Increasing Contribution of Chlorine Chemistry to Wintertime Ozone Formation Promoted by Enhanced Nitrogen Chemistry, Environ. Sci. Technol., 58, 22714–22721, https://doi.org/10.1021/acs.est.4c09523, 2024.
- Chen, Y.: Dataset for Molecular characterization of organic aerosol.xlsx, figshare [data set], https://doi.org/10.6084/m9.figshare.28956629.v1, 2025.
- Chen, Y., Takeuchi, M., Nah, T., Xu, L., Canagaratna, M. R., Stark, H., Baumann, K., Canonaco, F., Prévôt, A. S. H., Huey, L. G., Weber, R. J., and Ng, N. L.: Chemical characterization of secondary organic aerosol at a rural site in the southeastern US: insights from simultaneous high-resolution time-of-flight aerosol mass spectrometer (HR-ToF-AMS) and FIGAERO chemical ionization mass spectrometer (CIMS) measurements, Atmos. Chem. Phys., 20, 8421–8440, https://doi.org/10.5194/acp-20-8421-2020, 2020.
- Chen, Y., Yang, C., Xu, L., Chen, J., Zhang, Y., Shi, J., Fan, X., Zheng, R., Hong, Y., and Li, M.: Chemical composition of NR-PM₁ in a coastal city of Southeast China: Temporal variations and formation pathways, Atmos. Environ., 285, https://doi.org/10.1016/j.atmosenv.2022.119243, 2022.
- Chow, C., Watson, J., Lu, Z., Lowenthal, D., Frazier, C., Solomon, P., Thuillier, R., and Magliano, K.: Descriptive analysis of PM_{2.5} and PM₁₀ at regionally representative locations during SJVAQS/AUSPEX, Atmos. Environ., 30, 2079–2112, https://doi.org/10.1016/1352-2310(95)00402-5, 1996.
- Coward, E., Ohno, T., and Sparks, D.: Direct evidence for temporal molecular fractionation of dissolved organic matter at the

- iron oxyhydroxide interface, Environ. Sci. Technol., 53, 642–650, https://doi.org/10.1021/acs.est.8b04687, 2019.
- Cui, M., Li, C., Chen, Y., Zhang, F., Li, J., Jiang, B., Mo, Y., Li, J., Yan, C., Zheng, M., Xie, Z., Zhang, G., and Zheng, J.: Molecular characterization of polar organic aerosol constituents in offroad engine emissions using Fourier transform ion cyclotron resonance mass spectrometry (FT-ICR MS): implications for source apportionment, Atmos. Chem. Phys., 19, 13945–13956, https://doi.org/10.5194/acp-19-13945-2019, 2019.
- Cui, M., Han, Y., Yan, C., Zhang, F., Li, J., and Chen, Y.: Characteristics of polar organic compounds from diesel truck emissions measured by FT-ICR MS, Atmos. Environ., 319, 120319, https://doi.org/10.1016/j.atmosenv.2023.120319, 2024.
- Daellenbach, K., Cai, j., Hakala, S., Dada, L., Yan, C., Du, W., Yao,
 L., Zheng, F., Ma, J., Ungeheuer, F., Vogel, A., Stolzenburg, D.,
 Hao, Y., Liu, Y., Bianchi, F., Uzu, G., Jaffrezo, J., Worsnop, D.,
 Donahue N., and Kulmala, M.: Substantial contribution of transported emissions to organic aerosol in Beijing, Nat. Geosci., 17,
 747–754, https://doi.org/10.1038/s41561-024-01493-3, 2024.
- Du, M., Voliotis, A., Shao, Y., Wang, Y., Bannan, T. J., Pereira, K. L., Hamilton, J. F., Percival, C. J., Alfarra, M. R., and Mc-Figgans, G.: Combined application of online FIGAERO-CIMS and offline LC-Orbitrap mass spectrometry (MS) to characterize the chemical composition of secondary organic aerosol (SOA) in smog chamber studies, Atmos. Meas. Tech., 15, 4385–4406, https://doi.org/10.5194/amt-15-4385-2022, 2022.
- Du, Y., Che, H., Bao, Z., Liu, Y., Li, Q., Hu, M., Zhou, J., Zhang, S., Yao, X., Shi, Q., Chen, C., Han, Y., Meng, L., Long, X., Qi, X., He, C., and Chen, Y.: Characterization of Organosulfates (OSs) in typical urban areas in Eastern China: Source, Process, and Volatility, Atmos. Res., 301, 107258, https://doi.org/10.1016/j.atmosres.2024.107258, 2024.
- Ervens, B., Turpin, B. J., and Weber, R. J.: Secondary organic aerosol formation in cloud droplets and aqueous particles (aq-SOA): a review of laboratory, field and model studies, Atmos. Chem. Phys., 11, 11069–11102, https://doi.org/10.5194/acp-11-11069-2011, 2011.
- Faxon, C., Hammes, J., Le Breton, M., Pathak, R. K., and Hallquist, M.: Characterization of organic nitrate constituents of secondary organic aerosol (SOA) from nitrate-radical-initiated oxidation of limonene using high-resolution chemical ionization mass spectrometry, Atmos. Chem. Phys., 18, 5467–5481, https://doi.org/10.5194/acp-18-5467-2018, 2018.
- Frka, S., Sala, M., Kroflic, A., Hus, M., Cusak, A., and Grgic, I.: Quantum chemical calculations resolved identification of methylnitrocatechols in atmospheric aerosols, Environ. Sci. Technol., 50, 5526–5535, https://doi.org/10.1021/acs.est.6b00823, 2016.
- Haslett, S. L., Bell, D. M., Kumar, V., Slowik, J. G., Wang, D. S.,
 Mishra, S., Rastogi, N., Singh, A., Ganguly, D., Thornton, J.,
 Zheng, F., Li, Y., Nie, W., Liu, Y., Ma, W., Yan, C., Kulmala,
 M., Daellenbach, K. R., Hadden, D., Baltensperger, U., Prevot,
 A. S. H., Tripathi, S. N., and Mohr, C.: Nighttime NO emissions strongly suppress chlorine and nitrate radical formation during the winter in Delhi, Atmos. Chem. Phys., 23, 9023–9036,
 https://doi.org/10.5194/acp-23-9023-2023, 2023.
- Hong, Y., Xu, X., Liao, D., Liu, T., Ji, X., Xu, K., Liao, C., Wang,T., Lin, C., and Chen, J.: Measurement report: Effects of anthropogenic emissions and environmental factors on the forma-

- tion of biogenic secondary organic aerosol (BSOA) in a coastal city of southeastern China, Atmos. Chem. Phys., 22, 7827–7841, https://doi.org/10.5194/acp-22-7827-2022, 2022.
- Hong, Z., Zhang, H., Zhang, Y., Xu, L., Liu, T., Xiao, H., Hong, Y., Chen, J., Li, M., Deng, J., Wu, X., Hu, B., and Chen, X.: Secondary organic aerosol of PM_{2.5} in a mountainous forest area in southeastern China: Molecular compositions and tracers implication, Sci. Total Environ., 653, 496–503, https://doi.org/10.1016/j.scitotenv.2018.10.370, 2019.
- Huang, R. J., Zhang, Y., Bozzetti, C., Ho, K. F., Cao, J. J., Han, Y.,
 Daellenbach, K. R., Slowik, J. G., Platt, S. M., Canonaco, F., Zotter, P., Wolf, R., Pieber, S. M., Bruns, E. A., Crippa, M., Ciarelli, G., Piazzalunga, A., Schwikowski, M., Abbaszade, G., Schnelle-Kreis, J., Zimmermann, R., An, Z., Szidat, S., Baltensperger, U., El Haddad, I., and Prevot, A. S.: High secondary aerosol contribution to particulate pollution during haze events in China, Nature, 514, 218–222, https://doi.org/10.1038/nature13774, 2014.
- Huang, W., Saathoff, H., Shen, X., Ramisetty, R., Leisner, T., and Mohr, C.: Seasonal characteristics of organic aerosol chemical composition and volatility in Stuttgart, Germany, Atmos. Chem. Phys., 19, 11687–11700, https://doi.org/10.5194/acp-19-11687-2019, 2019.
- Huang, W., Wu, C., Gao, L., Gramlich, Y., Haslett, S. L., Thornton, J., Lopez-Hilfiker, F. D., Lee, B. H., Song, J., Saathoff, H., Shen, X., Ramisetty, R., Tripathi, S. N., Ganguly, D., Jiang, F., Vallon, M., Schobesberger, S., Yli-Juuti, T., and Mohr, C.: Variation in chemical composition and volatility of oxygenated organic aerosol in different rural, urban, and mountain environments, Atmos. Chem. Phys., 24, 2607–2624, https://doi.org/10.5194/acp-24-2607-2024, 2024.
- Junninen, H., Ehn, M., Petäjä, T., Luosujärvi, L., Kotiaho, T., Kostiainen, R., Rohner, U., Gonin, M., Fuhrer, K., Kulmala, M., and Worsnop, D. R.: A high-resolution mass spectrometer to measure atmospheric ion composition, Atmos. Meas. Tech., 3, 1039–1053, https://doi.org/10.5194/amt-3-1039-2010, 2010.
- Kawamura, K. and Bikkina, S.: A review of dicarboxylic acids and related compounds in atmospheric aerosols: Molecular distributions, sources and transformation, Atmos. Res., 170, 140–160, https://doi.org/10.1016/j.atmosres.2015.11.018, 2016.
- Koch, B. and Dittmar, T.: From Mass to Structure: An Aromaticity Index for High-Resolution Mass Data of Natural Organic Matter, Rapid Commun. Mass Spectrom., 20, 926–932, https://doi.org/10.1002/rcm.2386, 2006.
- Koch, B. and Dittmar, T.: From Mass to Structure: An Aromaticity Index for High-Resolution Mass Data of Natural Organic Matter. Rapid Commun. Mass Spectrom., 30, 250, https://doi.org/10.1002/rcm.7433, 2016.
- Kroll, J., Donahue, N., Jimenez, J., Kessler, S., Canagaratna, M., Wilson, K., Altieri, K., Mazzoleni, L., Wozniak, A., Bluhm, H., Mysak, E., Smith, J., Kolb C., and Worsnop, D.: Carbon Oxidation State as a Metric for Describing the Chemistry of Atmospheric Organic Aerosol, Nat. Chem., 3, 133–139, https://doi.org/10.1038/nchem.948, 2011.
- Lee, B. H., Lopez-Hilfiker, F., Mohr, C., Kurten, T., Worsnop, D., and Thornton. J.: An iodide-adduct high-resolution time-of-flight chemical-ionization mass spectrometer: Application to atmospheric inorganic and organic compounds, Environ. Sci. Technol., 48, 6309–6317, https://doi.org/10.1021/es500362a, 2014.

- Lee, B. H., Mohr, C., Lopez-Hilfiker, F. D., Lutz, A., Hallquist, M., Lee, L., Romer, P., Cohen, R. C., Iyer, S., Kurtén, T., Hu, W., Day, D. A., Campuzano-Jost, P., Jimenez, J. L., Xu, L., Ng, N. L., Guo, H., Weber, R. J., Wild, R. J., Brown, S. S., Koss, A., Gouw, J. de, Olson, K., Goldstein, A. H., Seco, R., Kim, S., McAvey, K., Shepson, P. B., Starn, T., Baumann, K., Edgerton, E. S., Liu, J., Shilling, J. E., Miller, D. O., Brune, W., Schobesberger, S., D'Ambro, E. L., and Thornton, J. A.: Highly functionalized organic nitrates in the southeast United States: Contribution to secondary organic aerosol and reactive nitrogen budgets, P. Natl. Acad. Sci. USA, 113, 1516–1521, https://doi.org/10.1073/PNAS.1508108113, 2016.
- Lim, Y. B., Tan, Y., Perri, M. J., Seitzinger, S. P., and Turpin, B. J.: Aqueous chemistry and its role in secondary organic aerosol (SOA) formation, Atmos. Chem. Phys., 10, 10521– 10539, https://doi.org/10.5194/acp-10-10521-2010, 2010.
- Lin, P., Rincon, A., Kalberer, M., and Yu, J.: Elemental composition of HULIS in the Pearl River Delta Region, China: Results inferred from positive and negative electrospray high resolution mass spectrometric data, Environ. Sci. Technol., 46, 7454–7462, https://doi.org/10.1021/es300285d, 2012.
- Lopez-Hilfiker, F. D., Mohr, C., Ehn, M., Rubach, F., Kleist, E., Wildt, J., Mentel, Th. F., Lutz, A., Hallquist, M., Worsnop, D., and Thornton, J. A.: A novel method for online analysis of gas and particle composition: description and evaluation of a Filter Inlet for Gases and AEROsols (FIGAERO), Atmos. Meas. Tech., 7, 983–1001, https://doi.org/10.5194/amt-7-983-2014, 2014.
- Lopez-Hilfiker, F. D., Mohr, C., D'Ambro, E. L., Lutz, A., Riedel, T. P., Gaston, C. J., Iyer, S., Zhang, Z., Gold, A., Surratt, J. D., Lee, B. H., Kurten, T., Hu, W. W., Jimenez, J., Hallquist, M., and Thornton, J. A.: Molecular composition and volatility of organic aerosol in the Southeastern U.S.: Implications for IEPOX derived SOA, Environ. Sci. Technol., 50, 2200–2209, https://doi.org/10.1021/acs.est.5b04769, 2016.
- Lopez-Hilfiker, F. D., Pospisilova, V., Huang, W., Kalberer, M., Mohr, C., Stefenelli, G., Thornton, J. A., Baltensperger, U., Prevot, A. S. H., and Slowik, J. G.: An extractive electrospray ionization time-of-flight mass spectrometer (EESI-TOF) for online measurement of atmospheric aerosol particles, Atmos. Meas. Tech., 12, 4867–4886, https://doi.org/10.5194/amt-12-4867-2019, 2019.
- Lu, C. Y., Wang, X. F., Dong, S. W., Zhang, J., Li, J., Zhao, Y. N., Liang, Y. H., Xue, L. K., Xie, H. J., Zhang, Q. Z., and Wang, W. X.: Emissions of fine particulate nitrated phenols from various on-road vehicles in China, Environ. Res., 179, 108709, https://doi.org/10.1016/j.envres.2019.108709, 2019a.
- Lu, C. Y., Wang, X. F., Li, R., Gu, R. R., Zhang, Y. X., Li, W. J., Gao, R., Chen, B., Xue, L. K., and Wang, W. X.: Emissions of fine particulate nitrated phenols from residential coal combustion in China, Atmos. Environ., 203, 10–17, https://doi.org/10.1016/j.atmosenv.2019.01.047, 2019b.
- Lu, C., Wang, X., Zhang, J., Liu, Z., Liang, Y., Dong, S., Li, M., Chen, J., Chen, H., Xie, H., Xue, L., and Wang, W.: Substantial emissions of nitrated aromatic compounds in the particle and gas phases in the waste gases from eight industries, Environ. Pollut., 283, 117132, https://doi.org/10.1016/j.envpol.2021.117132, 2021.
- Nah, T., Sanchez, J., Boyd, C. M., and Ng, N. L.: Photochemical Aging of α -pinene and β -pinene Secondary Organic Aerosol

- formed from Nitrate Radical Oxidation. Environ. Sci. Technol., 50, 222–231, https://doi.org/10.1021/acs.est.5b04594, 2016.
- Ng, N. L., Brown, S. S., Archibald, A. T., Atlas, E., Cohen, R. C., Crowley, J. N., Day, D. A., Donahue, N. M., Fry, J. L., Fuchs, H., Griffin, R. J., Guzman, M. I., Herrmann, H., Hodzic, A., Iinuma, Y., Jimenez, J. L., Kiendler-Scharr, A., Lee, B. H., Luecken, D. J., Mao, J., McLaren, R., Mutzel, A., Osthoff, H. D., Ouyang, B., Picquet-Varrault, B., Platt, U., Pye, H. O. T., Rudich, Y., Schwantes, R. H., Shiraiwa, M., Stutz, J., Thornton, J. A., Tilgner, A., Williams, B. J., and Zaveri, R. A.: Nitrate radicals and biogenic volatile organic compounds: oxidation, mechanisms, and organic aerosol, Atmos. Chem. Phys., 17, 2103–2162, https://doi.org/10.5194/acp-17-2103-2017, 2017.
- Nguyen, T., Lee, P., Updyke, K., Bones, D., Laskin, J., Laskin, A., and Nizkorodov, S.: Formation of nitrogen- and sulfur-containing light-absorbing compounds accelerated by evaporation of water from secondary organic aerosols, J. Geophys. Res.-Atmos., 117, https://doi.org/10.1029/2011JD016944, 2012.
- Noziere, B., Ekstrom, S., Alsberg, T., and Holmstrom, S.: Radical-initiated formation of organosulfates and surfactants in atmospheric aerosols, Geophys. Res. Lett., 37, https://doi.org/10.1029/2009GL041683, 2010.
- Peng, Y., Yuan, B., Yang, S., Wang, S., Yang, X., Wang, W., Li, J., Song, X., Wu, C., Qi, J., Zheng, E., Ye, C., Huang, S., Hu, W., Song, W., Wang, X., Wang, B., and Shao, M.: Photolysis frequency of nitrophenols derived from ambient measurements, Sci. Total Environ., 869, 161810, https://doi.org/10.1016/j.scitotenv.2023.161810, 2023.
- Putman, A., Offenberg, J., Fisseha, R., Kundu, S., Rahn, T., and Mazzoleni, L.: Ultrahigh-resolution FT-ICR mass spectrometry characterization of α-pinene ozonolysis SOA, Atmos. Environ., 46, 164–172, https://doi.org/10.1016/j.atmosenv.2011.10.003, 2012.
- Qi, J., Zheng, B., Li, M., Yu, F., Chen, C., Liu, F., Zhou, X., Yuan, J., Zhang, Q., and He, K.: A high-resolution air pollutants emission inventory in 2013 for the Beijing-Tianjin-Hebei region, China, Atmos. Environ., 170, 156–168, https://doi.org/10.1016/j.atmosenv.2017.09.039, 2017.
- Redman, A., Macalady, D., and Ahmann, D.: Natural organic matter affects arsenic speciation and sorption onto hematite, Environ. Sci. Technol., 36, 2889–2896, https://doi.org/10.1021/es0112801, 2002.
- Shang, Y., Li, L., Sun, T., Kong, X., Wang, S., and Hallquist M.: Characterization and Seasonal Variation of PM_{2.5} Composition in Xi'an, Northwest China: Oxygenated and Nitrogenous Organic Aerosol, ACS Earth Space Chem., 8, 1370–1384, https://doi.org/10.1021/acsearthspacechem.4c00042, 2024.
- Shen, J., Scholz, W., He, X.-C., Zhou, P., Marie, G., Wang, M., Marten, R., Surdu, M., Rörup, B., Baalbaki, R., Amorim, A., Ataei, F., Bell, D. M., Bertozzi, B., Brasseur, Z., Caudillo, L., Chen, D., Chu, B., Dada, L., Duplissy, J., Finkenzeller, H., Granzin, M., Guida, R., Heinritzi, M., Hofbauer, V., Iyer, S., Kemppainen, D., Kong, W., Krechmer, J. E., Kürten, A., Lamkaddam, H., Lee, C. P., Lopez, B., Mahfouz, N. G. A., Manninen, H. E., Massabò, D., Mauldin, R. L., Mentler, B., Müller, T., Pfeifer, J., Philippov, M., Piedehierro, A. A., Roldin, P., Schobesberger, S., Simon, M., Stolzenburg, D., Tham, Y. J., Tomé, A., Umo, N. S., Wang, D., Wang, Y., Weber, S. K., Welti, A., Wollesen de Jonge, R., Wu, Y., Zauner-Wieczorek, M., Zust,

- F., Baltensperger, U., Curtius, J., Flagan, R. C., Hansel, A., Möhler, O., Petäjä, T., Volkamer, R., Kulmala, M., Lehtipalo, K., Rissanen, M., Kirkby, J., El-Haddad, I., Bianchi, F., Sipilä, M., Donahue, N. M., and Worsnop, D. R.: High Gas-Phase Methanesulfonic Acid Production in the OH-Initiated Oxidation of Dimethyl Sulfide at Low Temperatures, Environ. Sci. Technol., 56, 13931–13944, https://doi.org/10.1021/acs.est.2c05154, 2022.
- Siegel, K., Karlsson, L., Zieger, P., Baccarini, A., Schmale, J., Lawler, M., Salter, M., Leck, C., Ekman, A., Riipinen I., and Mohr, C.: Insights into the molecular composition of semivolatile aerosols in the summertime central Arctic Ocean using FIGAERO-CIMS, Environ. Sci.-Atmos., 1, 161, https://doi.org/10.1039/d0ea00023j, 2021.
- Stark, H., Yatavelli, R. L. N., Thompson, S. L., Kang, H., Krechmer, J. E., Kimmel, J. R., Palm, B. B., Hu, W., Hayes, P. L., Day, D. A., Campuzano-Jost, P., Canagaratna, M. R., Jayne, J. T., Worsnop D. R., and Jimenez, J. L.: Impact of Thermal Decomposition on Thermal Desorption Instruments: Advantage of Thermogram Analysis for Quantifying Volatility Distributions of Organic Species, Environ. Sci. Technol., 51, 8491–8500, https://doi.org/10.1021/acs.est.7b00160, 2017.
- Sun, Y., Xu, W., Zhang, Q., Jiang, Q., Canonaco, F., Prévôt, A. S. H., Fu, P., Li, J., Jayne, J., Worsnop, D. R., and Wang, Z.: Source apportionment of organic aerosol from 2-year highly time-resolved measurements by an aerosol chemical speciation monitor in Beijing, China, Atmos. Chem. Phys., 18, 8469–8489, https://doi.org/10.5194/acp-18-8469-2018, 2018.
- Vidovic, K., Lasic Jurkovic, D., Sala, M., Kroflic, A., and Grgic, I.: Nighttime aqueous-phase formation of nitrocatechols in the atmospheric condensed phase, Environ. Sci. Technol., 52, 9722– 9730, https://doi.org/10.1021/acs.est.8b01161, 2018.
- Wan, Y., Huang, X., Jiang, B., Kuang, B., Lin, M., Xia, D., Liao, Y., Chen, J., Yu, J. Z., and Yu, H.: Probing key organic substances driving new particle growth initiated by iodine nucleation in coastal atmosphere, Atmos. Chem. Phys., 20, 9821–9835, https://doi.org/10.5194/acp-20-9821-2020, 2020.
- Wang, Y., Hu, M., Wang, Y., Zheng, J., Shang, D., Yang, Y., Liu, Y., Li, X., Tang, R., Zhu, W., Du, Z., Wu, Y., Guo, S., Wu, Z., Lou, S., Hallquist, M., and Yu, J. Z.: The formation of nitro-aromatic compounds under high NOx and anthropogenic VOC conditions in urban Beijing, China, Atmos. Chem. Phys., 19, 7649–7665, https://doi.org/10.5194/acp-19-7649-2019, 2019.
- Xia, M., Chen, X., Ma, W., Guo, Y., Yin, R., Zhan, J., Zhang, Y., Wang, Z., Zheng, F., Xie, J., Wang, Y., Hua, C., Liu, Y., Yan, C., and Kulmala, M.: Observations and Modeling of Gaseous Nitrated Phenols in Urban Beijing: Insights From Seasonal Comparison and Budget Analysis, J. Geophys. Res.-Atmos., 128, e2023JD039551, https://doi.org/10.1029/2023JD039551, 2023.
- Xie, M., Chen, X., Hays, M. D., Lewandowski, M., Offenberg, J., Kleindienst, T. E., and Holder, A. L.: Light absorption of secondary organic aerosol: composition and contribution of nitroaromatic compounds, Environ. Sci. Technol., 51, 11607– 11616, https://doi.org/10.1021/acs.est.7b03263, 2017.
- Xie, Q., Li, Y., Yue, S., Su, S., Cao, D., Xu, Y., Chen, J., Tong, H., Su, H., Cheng, Y., Zhao, W., Hu, W., Wang, Z., Yang, T., Pan, X., Sun, Y., Wang, Z., Liu, C., Kawamura, K., Jiang, G., Shiraiwa, M., and Fu P.: Increase of high molecular weight organosulfate with intensifying urban air pollution in the Megac-

- ity Beijing, J. Geophys. Res.-Atmos., 125, e2019JD032200, https://doi.org/10.1029/2019JD032200, 2020.
- Xin, X., Zhao, Y., Wan, Y., Zhang H., and Yu, H.: Molecular composition of organic aerosols in urban and marine atmosphere: A comparison study using FIGAERO-I-CIMS, ESI-FT-ICR MS, and GC × GC-EI-ToF-MS, Aerosol Sci. and Tech., 58, 1142–1156, https://doi.org/10.1080/02786826.2024.2377394, 2024.
- Xu, L., Guo, H., Weber R. J., and Ng, N. L.: Chemical Characterization of Water-Soluble Organic Aerosol in Contrasting Rural and Urban Environments in the Southeastern United States, Environ. Sci. Technol., 51, 78–88, https://doi.org/10.1021/acs.est.6b05002, 2017a.
- Xu, W., Han, T., Du, W., Wang, Q., Chen, C., Zhao, J., Zhang, Y., Li, J., Fu, P., Wang, Z., Worsnop, D., and Sun, Y.: Effects of Aqueous-Phase and Photochemical Processing on Secondary Organic Aerosol Formation and Evolution in Beijing, China, Environ. Sci. Technol., 51, 762–770, https://doi.org/10.1021/acs.est.6b04498, 2017b.
- Xu, W., Kuang, Y., Liang, L., He, Y., Cheng, H., Bian, Y., Tao, J., Zhang, G., Zhao, P., Ma, N., Zhao, H., Zhou, G., Su, H., Cheng, Y., Xu, X., Shao, M., and Sun, Y.: Dust-dominated coarse particles as a medium for rapid secondary organic and inorganic aerosol formation in highly polluted air, Environ. Sci. Technol., 54, 15710–15721, https://doi.org/10.1021/acs.est.0c07243, 2020.
- Yan, C., Nie, W., Äijälä, M., Rissanen, M. P., Canagaratna, M. R., Massoli, P., Junninen, H., Jokinen, T., Sarnela, N., Häme, S. A. K., Schobesberger, S., Canonaco, F., Yao, L., Prévôt, A. S. H., Petäjä, T., Kulmala, M., Sipilä, M., Worsnop, D. R., and Ehn, M.: Source characterization of highly oxidized multifunctional compounds in a boreal forest environment using positive matrix factorization, Atmos. Chem. Phys., 16, 12715–12731, https://doi.org/10.5194/acp-16-12715-2016, 2016.
- Yang, Y., Huang, L., Zhao, M., Wu, Y., Xu, Y., Li, Q., Wang, W., and Xue, L.: Multiphase reactions of organic peroxides and nitrite as a source of atmospheric organic nitrates, Nat. Commun., 16, 5437, https://doi.org/10.1038/s41467-025-60696-3, 2025.
- Ye, C., Yuan, B., Lin, Y., Wang, Z., Hu, W., Li, T., Chen, W., Wu, C., Wang, C., Huang, S., Qi, J., Wang, B., Wang, C., Song, W., Wang, X., Zheng, E., Krechmer, J. E., Ye, P., Zhang, Z., Wang, X., Worsnop, D. R., and Shao, M.: Chemical characterization of oxygenated organic compounds in the gas phase and particle phase using iodide CIMS with FIGAERO in urban air, Atmos. Chem. Phys., 21, 8455–8478, https://doi.org/10.5194/acp-21-8455-2021, 2021.

- Ye, Z., Hu, D., Wang, Z., Wang, H., and Ge, X.: Aqueous photochemical aging of water-soluble smoke particles from crop straws burning, Atmos. Environ., 40, 120897, https://doi.org/10.1016/j.atmosenv.2024.120897, 2025.
- Yu, L., Smith, J., Laskin, A., George, K. M., Anastasio, C., Laskin, J., Dillner, A. M., and Zhang, Q.: Molecular transformations of phenolic SOA during photochemical aging in the aqueous phase: competition among oligomerization, functionalization, and fragmentation, Atmos. Chem. Phys., 16, 4511–4527, https://doi.org/10.5194/acp-16-4511-2016, 2016.
- Zhang, M., Cai, D., Lin, Z., Liu, Z., Li, M., Wang, Y., and Chen, J.: Molecular characterization of atmospheric organic aerosols in typical megacities in China, npj Clim. Atmos. Sci., 7, 230, https://doi.org/10.1038/s41612-024-00784-1, 2024.
- Zhang, Y., Xu, L., Zhuang, M., Zhao, G., Chen, Y., Tong, L., Yang, C., Xiao, H., Chen, J., Wu, X., Hong, Y., Li, M., Bian, Y., and Chen, Y.: Chemical composition and sources of submicron aerosol in a coastal city of China: Results from the 2017 BRICS summit study, Sci. Total Environ., 741, 140470, https://doi.org/10.1016/j.scitotenv.2020.140470, 2020.
- Zhao, R., Mungall, E. L., Lee, A. K. Y., Aljawhary, D., and Abbatt, J. P. D.: Aqueous-phase photooxidation of levoglucosan a mechanistic study using aerosol time-of-flight chemical ionization mass spectrometry (Aerosol ToF-CIMS), Atmos. Chem. Phys., 14, 9695–9706, https://doi.org/10.5194/acp-14-9695-2014, 2014.
- Zheng, Y., Chen, Q., Cheng, X., Mohr, C., Cai, J., Huang, W., Shrivastava, M., Ye, P., Fu, P., Shi, X., Ge, Y., Liao, K., Miao, R., Qiu, X., Koenig, T., and Chen S.: Precursors and Pathways Leading to Enhanced Secondary Organic Aerosol Formation during Severe Haze Episodes, Environ. Sci. Technol., 55, 15680–15693, https://doi.org/10.1021/acs.est.1c04255, 2021.
- Zhou, W., Xu, W., Kim, H., Zhang, Q., Fu, P., Worsnop, D. R., and Sun, Y.: A review of aerosol chemistry in Asia: insights from aerosol mass spectrometer measurements, Environ. Sci. Process Impacts, 22, 1616–1653, https://doi.org/10.1039/d0em00212g, 2020.